Linearization improves the repeatability of quantitative Dynamic Contrast-Enhanced MRI

Kyle M. Jones[1] Marisa H. Borders,[2] Kimberly A. Fitzpatrick, [2]
Mark D. Pagel,[1,2] and Julio Cárdenas-Rodríguez[1-2]

1. Department of Biomedical Engineering, University of Arizona, Tucson, AZ
2. Department of Medical Imaging, University of Arizona, Tucson, AZ

Corresponding Author: Julio Cárdenas-Rodríguez, PhD
Department of Medical Imaging
1501 N. Campbell Ave.
Tucson, AZ, USA 85724-5024
Tel: +1-520-626-8305
Fax: +1-520-626-0395
Email: cardenaj@email.arizona.edu

Running Title: Repeatable DCE MRI with linear models

PeerJ Preprints | https://doi.org/10.7287/peerj.preprints.2824v1 | CC BY 4.0 Open Access | rec: 21 Feb 2017, publ: 21 Feb 2017

ABSTRACT

We studied the effect of linearization on the repeatability of the Tofts and reference region models (RRM) for Dynamic Contrast-Enhanced MRI (DCE MRI). We compared the repeatabilities of these two linearized models, the standard non-linear version, and semi-quantitative methods of analysis.

Simulated and experimental DCE MRI data from 12 rats with a flank tumor of C6 glioma acquired over three consecutive days were analyzed using four quantitative and semi-quantitative DCE MRI metrics. The quantitative methods used were: 1) Linear Tofts model (LTM), 2) Non-linear Tofts model (NTM), 3) Linear RRM (LRRM), and 4) Non-linear RRM (NRRM). The following semi-quantitative metrics were used: 1) Maximum enhancement ratio (*MER*), 2) time to peak (*TTP*), 3) initial area under the curve (*iauc64*), and 4) *slope*. LTM and NTM were used to estimate K^{trans}, while LRRM and NRRM were used to estimate K^{trans} relative to muscle (R^{Ktrans}). Repeatability was assessed by calculating the within-subject coefficient of variation (*wSCV*) and the percent intra-subject variation (*iSV*) determined with the Gage repeatability and reproducibility (R&R) analysis.

The *iSV* for R^{Ktrans} using LRRM was two-fold lower compared to NRRM at all simulated and experimental conditions. A similar trend was observed for the Tofts model, where LTM was at least 50% more repeatable than the NTM under all experimental and simulated conditions. The semi-quantitative metrics *iauc64* and *MER* were as equally reproducible as K^{trans} and R^{Ktrans} estimated by LTM and LRRM respectively. The *iSV* for *iauc64* and *MER* were significantly lower than the *iSV* for *slope* and *TTP*.

In simulations and experimental results, linearization improves the repeatability of quantitative DCE MRI by at least 30%, making it as repeatable as semi-quantitative metrics.

KEYWORDS:
Dynamic contrast-enhanced MRI
Repeatability
Reference Region Model
Pharmacokinetics
Linear models

PeerJ Preprints | https://doi.org/10.7287/peerj.preprints.2824v1 | CC BY 4.0 Open Access | rec: 21 Feb 2017, publ: 21 Feb 2017

1. INTRODUCTION

Dynamic contrast-enhanced MRI (DCE MRI) involves the serial acquisition of T_1-weighted images before, during, and after the injection of a contrast agent that shortens the T_1 relaxation time of water, resulting in an increase of the MRI signal in tissues/voxels where the agent accumulates.[1] After application of a proper pharmacokinetic (PK) model, parameters related to tissue perfusion,[2] blood flow,[3] capillary leakage,[4] and transit time of the contrast agent can be derived from the dynamic MRI signal in a voxel or a tissue of interest (TOI).[5]

The two PK parameters most commonly estimated from DCE MRI data are the rate of contrast agent transfer from to blood tissue (K^{trans}) and the rate of transfer from tissue to blood (k_{ep}).[1] Several studies have shown evidence that K^{trans} can be used to differentiate tumors from normal tissue,[6-7] and to monitor anti-cancer treatment in fibrosarcoma,[8] breast,[9-10] and brain neoplasms.[11-12]. Unfortunately, these results are inconsistent with other studies, which showed that K^{trans} offers little to no utility to monitor anti-cancer treatment in breast and brain cancers.[13-14] Because of these limitations, quantitative DCE MRI descriptors are not part of the standard of care for clinical DCE MRI.

These contradictory results may be due to the inherent insensitivity of DCE MRI that results in a low signal-to-noise ratio (SNR),[15-16] slow temporal resolution,[17] variability in the arterial input function (AIF) needed for PK modeling,[18-19] and/or the model assumed during data analysis.[20-21] Some of these limitations have been addressed by the introduction of the non-linear reference region model (NRRM),[22,23] which does not require AIF determination, and the linear reference region model (LRRM) that also does not require the AIF and gives more accurate parameter estimates than the NRRM under low SNR and slow temporal resolution.[24-25] The standard Tofts model for DCE MRI has also been linearized, and it was recently demonstrated that such linearization improves its performance under low SNR and low temporal resolution.[26]

We recently demonstrated that the relative K^{trans} (R^{Ktrans}) estimated by LRRM is a better predictor of response to neoadjuvant chemotherapy in breast cancer than the R^{Ktrans} estimated using NRRM. An analoguous behavior was observed for K^{trans} and k_{ep} estimated using the linear (LTM) and non-linear (NTM) Tofts models.[27] Based on these results, we hypothesized that linearization should improve the repeatability of quantitative DCE MRI. We performed a retrospective study to compare the repeatability of R^{Ktrans} and k_{ep} estimated by NRRM and LRRM. We also compared the repeatability of quantitative NRRM and LRRM descriptors with semi-quantitative descriptors and quantitative NTM and LTM descriptors of DCE MRI.

2. METHODS

All of the experimental data and MATLAB *R2015a* codes used in the simulations and experimental analyses are publicly available for download without restrictions.[28] The experimental data was downloaded from DataVerse,[21] while the code used to simulate and analyze all data is available at *https://github.com/JCardenasRdz/Gage-repeatability-DCE MRI*.

2.1 Theory of the quantitative analysis of DCE MRI and its models

The generalized kinetic model for DCE MRI establishes that the differential equation that describes the pharmacokinetic behavior of a contrast agent (CA) within a voxel is:

$$\frac{dC_{TOI}}{dt} = K^{trans} \cdot C_p(t) - k_{ep} C_{TOI} \qquad (1)$$

PeerJ Preprints | https://doi.org/10.7287/peerj.preprints.2824v1 | CC BY 4.0 Open Access | rec: 21 Feb 2017, publ: 21 Feb 2017

C_{TOI} is the concentration of the tracer in the tissue of interest (*TOI*) as a function of time. $C_p(t)$ is the concentration of the tracer in plasma as a function of time (also known as the AIF), and K^{trans} is the rate transfer constant from the plasma into the TOI, while k_{ep} is the transfer constant from the TOI to plasma. The quantitative analysis of DCE MRI data requires three steps to estimate K^{trans} and k_{ep} for any TOI: 1) solve Eq. [1], 2) transform the observed changes in the MRI signal to changes in concentration of the contrast agent, and 3) fit the concentration curves of step 2 to the solution obtained in step 1. The first and most common solution to Eq. [1] was developed by Tofts et al:[1]

$$C_{TOI}(t) = K^{trans} \cdot \int_0^T C_p(t) \cdot e^{-k_{ep}(T-t)} dt \quad (2)$$

Equation (2) depicts an equation that is non linear in the parameters, and requires a non-linear fitting routine to estimate K^{trans} and k_{ep}, thus we have named this method the Non-linear Tofts Model (NTM). Non-linear fitting methods are very sensitive to low SNR, while linear fitting methods are more robust and significantly faster. Murase, *et al.*, addressed these issues by developing a linear approximation of the NTM, and we have named this method the Linear Tofts Model (LTM) (Eq. [3]).[26]

$$C_{TOI}(t) = K^{trans} \cdot \int_0^T C_p(t)\,dt - k_{ep} \cdot \int_0^T C_{TOI}(t)\,dt \quad (3)$$

Requiring to know the $C_p(t)$ is a major limitation of Eq. [2] and Eq. [3], because it is challenging to measure $C_p(t)$ experimentally. The reference region model (RRM) was introduced to remove the need of knowing $C_p(t)$, and uses instead a reference region (RR) as surrogate for the $C_p(t)$ (Eq. [4]).[22,29]

$$C_{TOI}(t) = \frac{K^{trans,TOI}}{K^{trans,RR}} \cdot C_{RR}(t) + \frac{K^{trans,TOI}}{K^{trans,RR}} \cdot [k_{ep,RR} - k_{ep,TOI}] \cdot \int_0^T C_{RR}(t) \cdot e^{-kep,TOI(T-t)} dt \quad (4a)$$

$$C_{TOI}(t) = R^{Ktrans} C_{RR}(t) + R^{Ktrans} \cdot [k_{ep,RR} - k_{ep,TOI}] \cdot \int_0^T C_{RR}(t) \cdot e^{-kep,TOI(T-t)} dt \quad (4b)$$

$C_{TOI}(t)$ and $C_{RR}(t)$ are the concentrations of the contrast agent at time t in the TOI and RR respectively. $K^{trans,TOI}$ and $K^{trans,RR}$ are the transfer constants between plasma and the extravascular extracellular space (EES) of the TOI and the RR respectively. $R^{Ktrans} = K^{trans,TOI} / K^{trans,RR}$, $k_{ep,RR}$ and $k_{ep,TOI}$ are the transfer rates (min^{-1}) from the TOI and RR back to the plasma. Estimating R^{Ktrans}, $k_{ep,RR}$ and $k_{ep,TOI}$ using Eq. [4] requires a nonlinear fitting method. Thus, we have named Eq. [4] the Non-linear RRM (NRRM). We obtained a linear solution to the RRM, and demonstrated that the Linear RRM (LRRM) is more robust than NRRM to low SNR and slow temporal resolution (Eq. [5]).[24]

$$C_{TOI}(t) = R^{Ktrans} \cdot C_{RR}(t) + \frac{K^{trans,TOI}}{v_{e,RR}} \cdot \int_0^T C_{RR}(t)\,dt - k_{ep,TOI} \cdot \int_0^T C_{TOI}(t)\,dt \quad (5)$$

PeerJ Preprints | https://doi.org/10.7287/peerj.preprints.2824v1 | CC BY 4.0 Open Access | rec: 21 Feb 2017, publ: 21 Feb 2017

The same definitions used for Eq. [4] apply to Eq. [5], and $v_{e,RR}$ is the fractional volume of the extravascular extracellular space. The goal of our study was to determine how the model used in the analysis of the data affects the repeatability of DCE MRI.

2.2 Gage Repeatability and Reproducibility (R&R) analysis

The Gage Repeatability and Reproducibility (Gage R&R) methodology was initially developed to determine the sources of variation in a manufacturing system.[30] Gage R&R analysis uses ANOVA to determine the percent of the observed variation in a system that is due to the parts (process), measuring protocol (repeatability), and the operator (reproducibility). Thus, this methodology can be used to determine if the inherent variability in the system is small compared to the process variability, and the proportion of the observed variability caused by differences in operators. The Gage R&R study of DCE MRI data presented in this work used repeated imaging sessions on the same subject (part) to determine the percentage of the observed variability that is due to the fitting algorithm used for the analysis of DCE MRI data. The Gage R&R methodology was implemented using the *gagerr* function in Matlab R2015a.[28]

2.3 Simulations

Thirty simulated tumor enhancement curves were created by using K^{trans} and v_e values that were randomly selected from a normal distribution (Figure 1). The mean K^{trans} was set to 0.25 min^{-1} with a standard deviation of 0.1, and the mean v_e was set to 0.4 with a standard deviation of 0.1. A single muscle reference region enhancement curve was created for all subsequent analyses using a K^{trans} of 0.1 min^{-1} and a v_e of 0.1. These values represented reasonable values for tumor and muscle tissues from previous reports.[31] All curves were simulated using Eq. [2], and a simulated *Cp(t)* was simulated (Eq. [6]):

$$C_p(t) = A \cdot t \cdot e^{(-t \cdot C)} + D \cdot (1 - e^{-t \cdot E}) \cdot e^{-t \cdot F} \quad (6)$$

where A = 30 mM/min, C = 4.0 min^{-1}, D = 0.65 mM, E = 5.0 min, and F = 0.04 min^{-1} . This set of parameters simulated an AIF with an injection speed of 0.005 mL/sec, which is similar to a previously reported AIF.[32]

To simulate potential changes in enhancement curves under experimental conditions of performing DCE MRI of a rat tumor model for 3 consecutive days, white Gaussian noise was added to each of the 30 simulated enhancement curves 3 separate times at the same SNR. White Gaussian noise was also added to a simulated muscle reference region enhancement curve. SNR was defined as the ratio of the signal power over the noise power in decibels.

The R^{Ktrans} value for each of the 3 curves for each of the 12 rats over three consecutive days was determined using LRRM without a non-negative constraint; LRRM with a non-negative constraint; and NRRM with a non-negative constraint and initial guesses for R^{Ktrans} taken from a gamma distribution with coefficient a = 1.40 and b = 0.56, which corresponds to reasonable values from previous reports (NRRM); and NRRM with a non-negative constraint and initial guesses for R^{Ktrans}, $k_{ep,TOI}$, and $k_{ep,RR}$ taken from the estimates from LRRM with a non-negative constraint (NRRM*). Additionally, we determined the rate of transfer from tissue to blood in the tissue of interest ($k_{ep,TOI}$), and the rate of transfer from tissue to blood in the reference region ($k_{ep,RR}$).

PeerJ Preprints | https://doi.org/10.7287/peerj.preprints.2824v1 | CC BY 4.0 Open Access | rec: 21 Feb 2017, publ: 21 Feb 2017

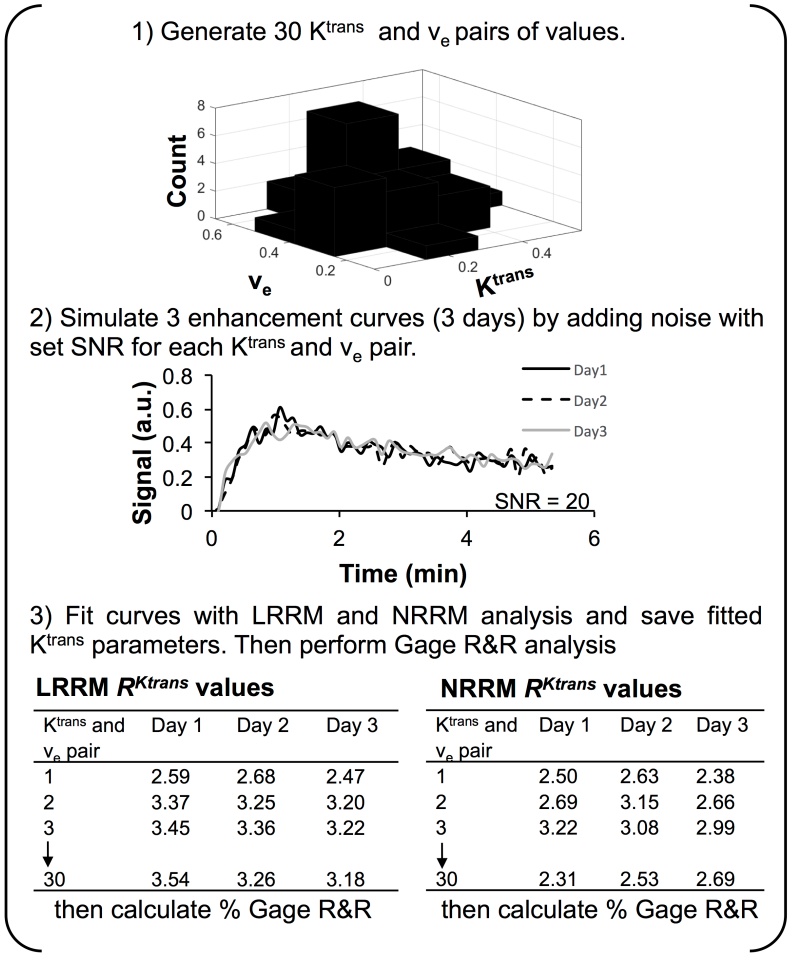

Figure 1. A diagram of the steps to produce simulated Gage R&R percentage plots. 1) 30 K^{trans} and v_e values were generated from a normal distribution. K^{trans} mean = 0.25 and standard deviation = 0.1. v_e mean = 0.4 and standard deviation = 0.1. The K^{trans} and v_e values were paired and the Tofts model was used to simulate 30 enhancement curves. To simulate how DCE MRI data from a single mouse could fluctuate over 3 days, 2) white Gaussian noise (SNR = 20 in this example) was added to an individual enhancement curve 3 times. 3) Each curve with noise was fit by NRRM, LRRM, LTM, and NTM analysis and the fitted R^{Ktrans} and K^{trans} values were stored in their respective tables. This process was repeated for all 30 enhancement curves. After, Gage R&R analysis was conducted and the percent variance (repeatability) value was stored. Steps 1-3 were repeated 1000 times using the same SNR, and the percent variance values were stored each time. After, the median value of the 1000 % variance values generated was taken as the true % variance for the particular SNR.

Gage R&R analysis was performed to measure the repeatability of the R^{Ktrans} values determined with LRRM, NRRM, and NRRM* through the calculation of percent intra-group variances due to the fitting method. These three values were stored and the process starting from the addition of white Gaussian noise was repeated 1000 times. The median Gage R&R percent variance values from the 1000 values generated for each of the three fitting methods were taken as the true Gage R&R percent variance values for that SNR. The process was repeated for SNR

PeerJ Preprints | https://doi.org/10.7287/peerj.preprints.2824v1 | CC BY 4.0 Open Access | rec: 21 Feb 2017, publ: 21 Feb 2017

values ranging from 5 to 40. Quantitative LTM and NTM analyses and semi-quantitative analyses were also performed in the same manner.

2.4 *In vivo* study

2.4.1 Animal Model

As described previously, all experimental data for this study was obtained from DataVerse.[21] The Institutional Animal Care and Use Committee of the University of Texas MD Anderson Cancer Center approved the studies. Twelve male Cr1:NIH-Foxn1^{rnu} T cell deficient, athymic nude rats (Charles River, Wilmington, MA) were injected subcutaneously with 5000 C6 rat glioma cells in the flank region. Tumor diameters were monitored daily with calipers until they reached 1 cm. At that time, the rats were imaged on 3 consecutive days with DCE MRI.

At the start of each MRI scanning session, hair around the tumor region was shaved and the tumor was placed in a bath of ultrasound gel to improve B_0 homogeneity around the tumor. Isoflurane gas (1-2% in a 1 l/min O_2 flow) was used to anesthetize the rat and a temperature controlled pad was placed underneath the rat to maintain temperature. A tail vein was catheterized to deliver the contrast agent.

2.4.2 DCE MRI Acquisition Methods

All imaging was conducted with a 7 T Bruker MRI scanner with a 30 cm bore. Sagittal and axial T_2 weighted images and axial T_1 weighted images were used to locate the tumor. A 3D fast spoiled gradient echo sequence was used for DCE MRI. Axial images were acquired using a 10 msec repetition time (TR), 1.7 msec echo time (TE), 15^o excitation pulse, 16 mm slab thickness (8 slices each 2 mm thick), 469 x 625 µm in-plane resolution, 128 x 80 matrix size, 60 x 50 mm field of view and 1 average. A spoiled hermite magnetization preparation pulse was used to excite an 8 cm slab 2 mm caudal to the DCE MRI slice package to reduce inflow artifacts. 50 frames of images were acquired with a temporal resolution of 6.4 sec and a total scan time of 320 sec.

After 10 baseline images were acquired, a bolus of 0.2 mmol/kg of gadopentetate dimeglumine (Gd-DTPA, Bayer Healthcare Pharmaceuticals, Wayne, NJ) was delivered at an injection rate of 0.005 mL/sec followed by a saline flush of the same volume and injection rate. Two of the twelve rats had technical scanning failures on 1 of the 3 days of imaging. As a result, 3 consecutive DCE MRI studies were not obtained for these rats. Data from these 2 rats were excluded from analysis.

2.4.3 Image Analysis

Because a quantitative pre-contrast T_1 map was not obtained, we used the signal enhancement ratio (*SER*) to replace concentration in the equations. The *SER* and concentration are linearly correlated (Eq. [7]):

$$SER(t) = \frac{S_{(t)} - S_{(0)}}{S_{(0)}} \quad (7)$$

Where *SER*(t) is the *SER* at time *t*, *S(t)* is the MR signal at time *t*, and *S(0)* is the signal before injection of the contrast agent (*t*=0).

The following semi-quantitative metrics were used in this work: a) maximum enhancement ratio (*MER*), b) time to peak (*TTP*), c) initial area under the curve (*iauc64*), and d) *slope* (Figure 2). The *MER* was defined as the maximum of each *SER(t)* curve. The *TTP* was determined by subtracting the time at the final baseline time point (10th image) from the time of

PeerJ Preprints | https://doi.org/10.7287/peerj.preprints.2824v1 | CC BY 4.0 Open Access | rec: 21 Feb 2017, publ: 21 Feb 2017

the *MER*. *iacu64* was determined from the area under the curve from the first post-baseline time point (11th image) to the time point acquired 64 seconds post-baseline (20th image). The slope was determined by dividing *MER* by *TTP*.

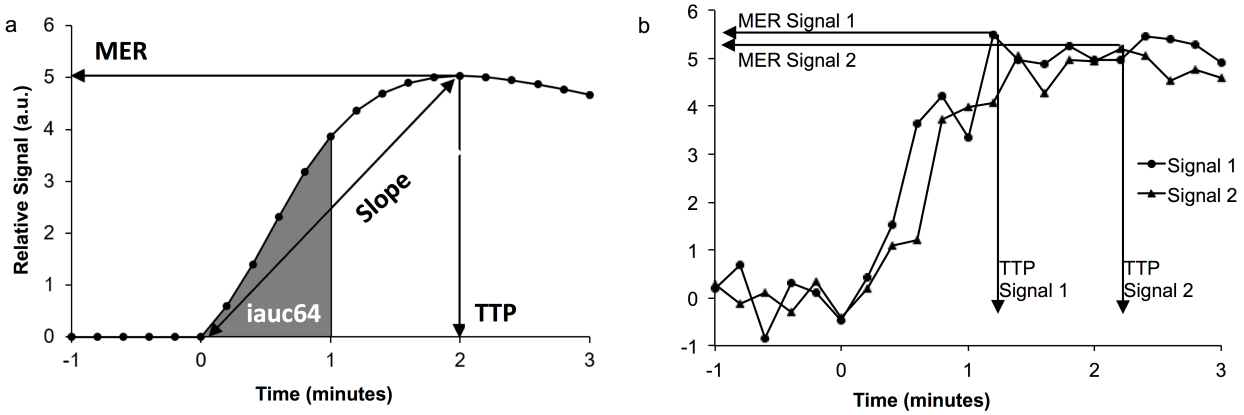

Figure 2. Semi-quantitative analyses. a) Mean Enhancement Ratio (*MER*) is the maximum of the curve, Time To Peak (*TTP*) is the time from the last baseline image (0 minutes) to the time at the maximum (2.0 minutes), *slope* is *MER* divided by *TTP*, and *iauc64* is the area under the curve from the last baseline image to 64 seconds post-baseline (shaded area). b) *TTP* is affected by noise more than *MER*.

Data fitting

As mentioned earlier, the NTM and NRRM require a non-linear fitting algorithm and an initial guess to estimate their respective pharmacokinetic parameters. An initial guess of K^{trans} = 0.5, and $k_{ep,TOI}$ = 5.0 was used for the NTM, while the following initial guesses were used for the NRRM: R^{Ktrans}=2.0, $k_{ep,TOI}$= 5.0, and $k_{ep,RR}$= 5.0. The MATLAB function *lsqcurvefit* was used for all non-linear fittings, while constraining all possible solutions between 0 and 10. The function tolerance was set to 1 x 10^{-16} and the maximum number of iterations was set to 100,000. The linear methods do not require an initial guess, but their solution was constrained to be greater than or equal to zero using non-negative least squares as implemented in the MATLAB function *lsqnonneg*. Finally, we studied the effect of using the parameters estimated with the LTM as the initial guess for the NTM (NTM*), and the parameters estimated by the LRRM as the initial guess for the NRRM (NRRM*).

Our quantitative analysis of all DCE MRI data using the NTM (Eq. [2]) and LTM (Eq. [3]) assumed a population AIF of the form:

$$C_p(t) = 0.64 \cdot e^{-0.033 \cdot t} + 0.42 \cdot e^{-0.0010 \cdot t} \quad (6)$$

The fitting for the NRRM and LRRM used muscle as a surrogate for the AIF.

Region of interest (ROI) approach

ROI Analysis

ROIs for the tumor and muscle were drawn by a single observer (KMJ) on slices 4, 5, and 6 of the 8 slices imaged for each rat. The three slices chosen showed the largest tumor volume. The same ROIs for any given rat were used for LTM, NTM, LRRM and NRRM analyses. For each rat, the average intensity of the whole tumor ROI and muscle reference region ROI from all time points were used to generate the enhancement curve that was fit with LRRM and NRRM

PeerJ Preprints | https://doi.org/10.7287/peerj.preprints.2824v1 | CC BY 4.0 Open Access | rec: 21 Feb 2017, publ: 21 Feb 2017

analyses to compute R^{Ktrans}, $k_{ep,TOI}$, and $k_{ep,RR}$. The average signal intensity of the whole tumor ROI and the population AIF were used for the LTM and NTM analyses.

Pixelwise Analysis

For an individual rat, each pixel within the ROI chosen for the tumor region was used to compute R^{Ktrans}, $k_{ep,TOI}$, and $k_{ep,RR}$. A single enhancement curve for the muscle reference region, generated by taking the average intensity value of the whole muscle reference region ROI from all time points, was used for all tumor pixel analysis. Based on the SNR of these data sets, pixels within the tumor ROI that showed less than 10% enhancement were excluded from analysis. This was also done in a previous study that used this data.[21] Additionally, pixels that showed poor fits based on the R^2 value were excluded from analysis. A range of R^2 values from 0 – 0.9 were used as the cutoff point to ensure that comparisons between LRRM and NRRM were not affected by the selected R^2 cutoff point. After removing the pixels with poor fits, the median value of the remaining pixels was determined for R^{Ktrans}, $k_{ep,TOI}$, and $k_{ep,RR}$.

2.4.4 Statistical Analysis

A summary of the parameter values generated from quantitative and semi-quantitative DCE MRI analyses were provided in the form of mean, range, and within-subject coefficient of variation (wSCV). The values were taken on a global scale meaning that values from all rats over each of the three time points were included in the calculation. The wSCV was calculated as follows: 1) the base-10 logarithm was applied to estimated quantitative and semi-quantitative descriptors, 2) the within-subject variance (variance for each row) was calculated, 3) the mean within-subject standard deviation was calculated (wSD) by taking the square root of the within-subject variance, 4) wsCV= 1-antilog(wSD)-1.[33,34] A Student's t-Test at the 95 % confidence level was used to determine the level of significance of the differences between LRRM and NRRM with R^{Ktrans} and $k_{ep,TOI}$.

Gage R&R analysis was also performed to test repeatability.[29] Normally, Gage R&R analysis is conducted to test variations between operators measuring a specific characteristic of a part. It is of course desired that different operators would measure the same value for the same part. Gage R&R analysis allows for the measurement of the percent variation in the measured quantity due to the operator compared to the total variation. In this study, we compared different fitting methods rather than comparing different operators. Thus, each fitting method was assigned a unique operator identification and each rat was given a unique part identification for Gage R&R analysis. As a result, the intra-part or intra-subject percent variance (*iSV)* measured was due to the fitting method. This analysis was performed for both the simulations and the experimental data.

3. RESULTS

3.1 Simulations

A total of 5 hours 32 minutes of computation time were required to generate 3.15 million simulated enhancement curves. These curves were subsequently analyzed with quantitative and semi-quantitative methods, and then with Gage R&R analysis. The use of 30 enhancement curves was sufficient for convergence as evidenced by the tight confidence intervals in the Gage R&R plots (Figure 3). The median percent variance due to repeatability was obtained from the 1000 Gage R&R analyses performed at each SNR (Figure 3). The median percent variance value and its corresponding 95% confidence interval were evaluated over the range of SNRs tested from each DCE MRI fitting method. Comparisons between LRRM with and without non-

PeerJ Preprints | https://doi.org/10.7287/peerj.preprints.2824v1 | CC BY 4.0 Open Access | rec: 21 Feb 2017, publ: 21 Feb 2017

negative constraints showed no difference in percent variance over the range of SNRs tested (Figure 3A). Thus, LRRM with a non-negative constraint was chosen to compare with NRRM, which also had a non-negative constraint, to avoid erroneous negative R^{Ktrans}, $k_{ep,TOI}$, and $k_{ep,RR}$ values from being generated in both methods.

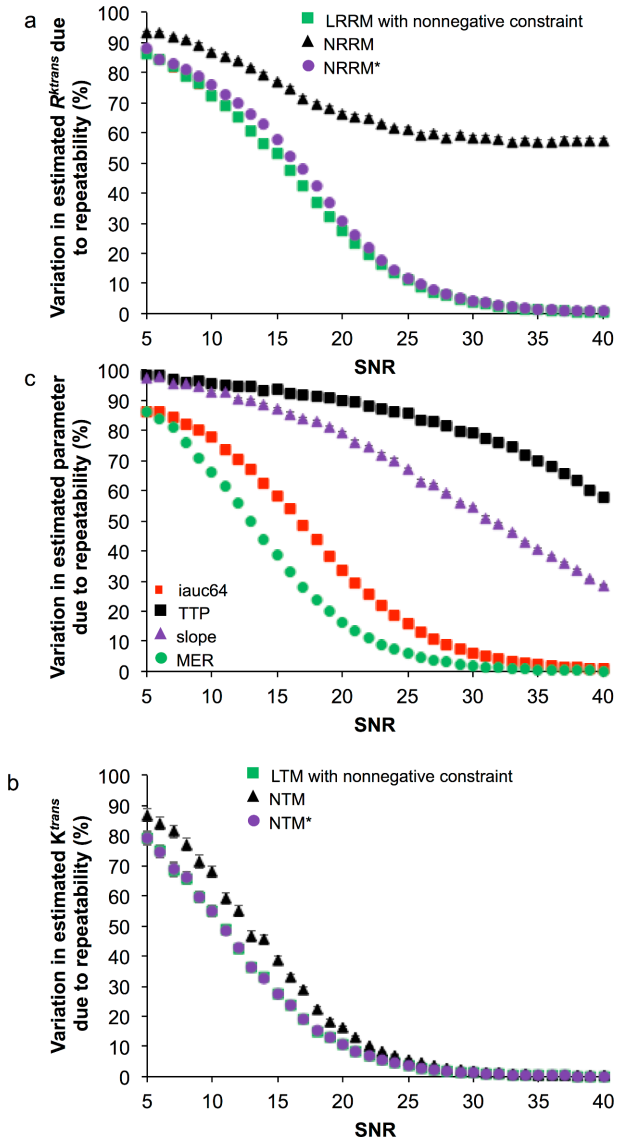

Figure 3. Dependence of Gage R&R on signal-to-noise. The median Gage R&R percent of the 1000 repetitions (described in Figure 1) is displayed for each SNR tested for a) quantitative reference region analyses, b) semi-quantitative analyses, and c) quantitative Tofts analyses. The LRRM analysis without and with a non-negative constraint produced almost identical Gage R&R percentages. Also note that the 95% CIs were smaller than the marker size for most plots.

LRRM showed a significantly lower Gage R&R percent variance compared to NRRM at all SNRs tested (Figure 3A). A significant difference was defined as non-overlapping 95% confidence intervals. Interestingly, when repeating the analysis with NRRM* (NRRM initialized

PeerJ Preprints | https://doi.org/10.7287/peerj.preprints.2824v1 | CC BY 4.0 Open Access | rec: 21 Feb 2017, publ: 21 Feb 2017

using LRRM-derived coefficients as the initial guess), the Gage R&R percent variance values were similar between LRRM and NRRM* (Figure 3A). This result emphasizes that the repeatability of R^{Ktrans} estimated via the NRRM is highly dependent on a proper initial guess.

LTM showed a significantly lower Gage R&R percent variance compared to NTM and LRRM at low SNRs (Figure 3B). The significant difference between LTM and NTM at low SNRs further emphasizes that linearizing a model improves repeatability. Additionally, when repeating analysis with NTM* (NTM initialized using LTM-derived coefficients as initial guesses), the Gage R&R percent variance values were similar between LTM and NTM, which was seen with LRRM and NRRM as well. Semi-quantitative analyses showed the best repeatability measurements with *iauc64* and *MER* (Figure 3C). The variability of these two descriptors was significantly lower than the variability of the *slope* and *TTP* at all SNRs, and similar to the R^{Ktrans} values estimated via the *LRRM* and *NRRM**. The Gage R&R value of the *slope* was significantly lower than for *TTP* at all SNRs and similar to NRRM with a random initial guess at mid-range SNRs.

3.2 *In vivo* Results

Overall, the semi-quantitative measurements, LTM, and LRRM measurements showed lower wSCVs than the NRRM measurements, with *TTP* showing the lowest wSCV in both pixelwise and ROI analyses (Table 1). Notably, the wSCVs of R^{Ktrans} measurements were lower with LRRM vs. NRRM in pixelwise analysis. The wSCVs of R^{Ktrans} measurements were also lower with NRRM* vs. NRRM in pixelwise analysis. The R^{Ktrans} values from all rats at all time points were significantly higher with LRRM compared to NRRM in pixelwise ($p<0.01$) and ROI analysis ($p<0.01$) and the $k_{ep,TOI}$ values were significantly lower with LRRM compared to NRRM in both pixelwise ($p<0.01$) and ROI analysis ($p < 0.01$). The R^{Ktrans} values were significantly higher with NRRM* compared to NRRM in pixelwise analysis ($p = 0.04$) and the $k_{ep,TOI}$ values were significantly lower with NRRM* compared to NRRM in pixelwise analysis ($p < 0.01$).

Interestingly, the R^{Ktrans} and the $k_{ep,TOI}$ values from ROI analysis were similar between NRRM* and NRRM. This was also seen in the K^{trans} and the $k_{ep,TOI}$ values from ROI analysis between NTM* and NTM. Therefore data with high SNR produces the same estimates for the quantitative metrics produced by reference region and Tofts model analyses regardless of the initial guess. Pixelwise analysis however showed similar R^{Ktrans} and $k_{ep,TOI}$ values between NRRM* and LRRM. This suggests that using the initial guesses produced by LRRM for NRRM analysis results in similar estimates for R^{Ktrans} and $k_{ep,TOI}$ with data that has low SNR. This similarity is based on median values produced by LRRM and NRRM*, and comparing individual pixel fits between NRRM and NRRM* may not always be similar. Thus, using good initial guesses is more beneficial for data with low SNR than data with high SNR.

For Gage R&R analysis of the experimental DCE MRI study, only a single percent variance value is generated for the dataset, meaning statistical significance could not be assessed (Table 2).

PeerJ Preprints | https://doi.org/10.7287/peerj.preprints.2824v1 | CC BY 4.0 Open Access | rec: 21 Feb 2017, publ: 21 Feb 2017

Table 1. Results of DCE MRI Analyses

		ROI			Pixel		
Model	**Parameter**	**Mean**	**IQR**	**wSCV**	**Mean**	**IQR**	**wSCV**
Quantitative Parameters (Reference Region)							
LRRM	R^{Ktrans}	2.57	1.86-3.23	0.41	2.40	1.67-3.16	0.40
	$k_{ep,TOI}$	0.11	0.01-0.73	0.74	0.03	0.0-0.04	0.68
NRRM	R^{Ktrans}	1.52	1.02-2.61	0.97	1.99	1.13-2.97	0.92
	$k_{ep,TOI}$	1.03	0.62-1.47	0.91	1.33	0.81-1.55	0.73
NRRM*	R^{Ktrans}	1.24	0.73-1.68	0.74	1.99	1.13-2.97	0.63
	$k_{ep,TOI}$	0.45	0.12-0.71	0.61	0.30	0.07-0.43	0.53
Quantitative Parameters (Tofts Model)							
LTM	K^{trans}	0.25	0.03-0.34	0.43	0.22	0.09-0.24	0.66
	$k_{ep,TOI}$	0.85	0.64-1.10	0.37	0.90	0.73-1.05	0.21
NTM	K^{trans}	0.16	0.09-0.24	0.57	0.18	0.17-0.21	0.20
	$k_{ep,TOI}$	7.64	6.89-8.04	0.19	8.20	8.67-9.48	0.45
NTM*	K^{trans}	0.08	0.05-0.11	0.43	0.05	0.04-0.05	0.27
	$k_{ep,TOI}$	1.87	1.04-2.32	0.26	2.21	1.59-2.83	0.29
Semi-Quantitative Parameters							
	MER	5.93	4.56 – 8.22	0.44	7.46	6.22 – 8.81	0.25
	TTP	3.79	3.20 – 4.05	0.15	3.09	2.99 – 3.20	0.07
	iauc64	0.21	0.15 – 0.29	0.48	0.22	0.18 – 0.26	0.29
	slope	1.56	1.31 – 2.60	0.41	2.46	2.13 – 2.82	0.27

LRRM = linear reference region model
NRRM = nonlinear reference region model with set initial guess
NRRM* = nonlinear reference region model with initial guess from LRRM estimates
LTM = linear tofts model
NTM = nonlinear tofts model with set initial guess
NTM* = nonlinear tofts model with initial guess from LTM estimates
MER = mean enhancement ratio, TTP = time to peak, iauc64 = initial area under the curve
IQR: inter-quartile range
wSCV: within subject coefficient of variation. Bounds: 95% lower and upper confidence intervals

PeerJ Preprints | https://doi.org/10.7287/peerj.preprints.2824v1 | CC BY 4.0 Open Access | rec: 21 Feb 2017, publ: 21 Feb 2017

Table 2. Summary of Gage R&R Percent Variances

	Pixelwise Analysis	ROI Analysis
Reference Region Model		
LRRM	45.1	65.7
NRRM	78.3	93.5
NRRM*	53.3	86.7
Tofts Model		
LTM	59.5	62.4
NTM	86.9	84.3
NTM*	62.7	71.8
Semi-Quantitative		
MER	46.1	65.5
Slope	50.9	48.2
TTP	88.7	100
iauc64	46.5	66.4

Similar to simulation results, the median Gage R&R percent variance value from analysis was lower with LRRM compared to NRRM and lower with LTM compared to NTM in both pixelwise and ROI analysis. This held true for all thresholds set for pixel inclusion based on the R^2 of the fit (Figure 4A and 4B). An R^2 value of 0.9 was not chosen as a threshold because of the high number of pixels that were discarded when doing so. The median Gage R&R percent variance value was lower with NRRM* compared to NRRM and NTM* compared to NTM for pixelwise analysis but similar for ROI analysis, which matched with wSCV results. The Gage R&R percent variance value for R^{Ktrans} with LRRM was similar to percent variance values for LTM, *MER*, *slope*, and *iauc64* in both pixelwise and ROI analysis (Table 2). The Gage R&R percent variance values for R^{Ktrans} with NRRM, NTM, and *TTP* were similar, and were also higher than all other Gage R&R percent variance values in both pixelwise and ROI analysis. We attribute the lower repeatability of *TTP* to the stronger dependence of *TTP* on image noise relative to the dependence of *MER* and *iauc64* on image noise (Figure 2B).

R^{Ktrans} pixelwise maps from a representative rat over the three days of DCE MRI show the distribution of R^{Ktrans} values with LRRM, NRRM, and NRRM* (Figure 5). The median R^{Ktrans} values from the maps for days 1, 2, and 3 were 3.44, 3.08, and 3.16 min^{-1} respectively for LRRM; 3.52, 1.26, and 3.17 min^{-1} respectively for NRRM; and 3.51, 2.89, and 2.97 min^{-1} respectively for NRRM*. These results indicated a larger variability with NRRM as compared to LRRM and NRRM* in measuring R^{Ktrans} over multiple days. Additionally, the pixelwise distributions for NRRM had larger standard deviations and were more highly skewed than the

PeerJ Preprints | https://doi.org/10.7287/peerj.preprints.2824v1 | CC BY 4.0 Open Access | rec: 21 Feb 2017, publ: 21 Feb 2017

pixelwise distributions with LRRM. For the rat shown in Figure 5, the standard deviation of the pixels for days 1, 2, and 3 were 2.0, 2.16, and 2.63 respectively for LRRM; 2.50, 0.84, and 2.97 respectively for NRRM; and were 2.22, 1.87, and 2.31 respectively for NRRM*.

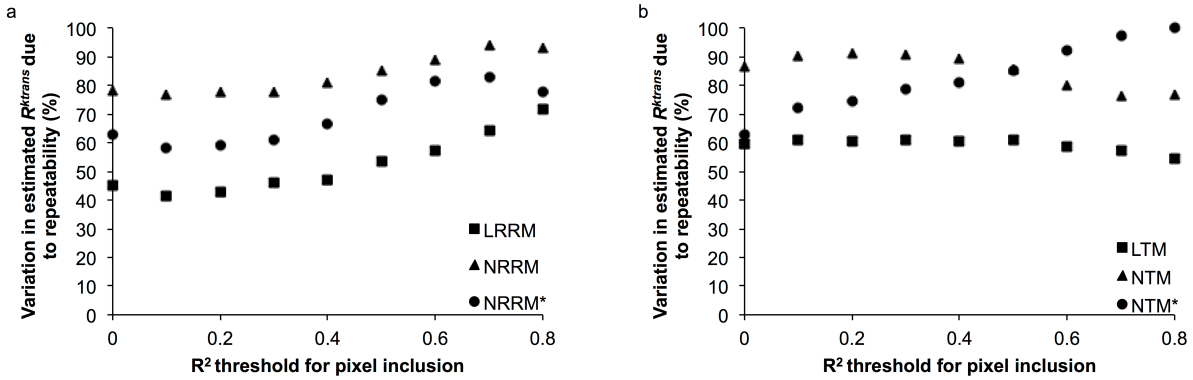

Figure 4. *In vivo* pixelwise percent Gage R&R plots. a) LRRM, NRRM, and NRRM* and b) LTM, NTM, and NTM* Gage R&R percent variances by pixelwise analysis as a function of the R^2 correlation coefficient of the fit. Pixels that had R^2 coefficients less than the threshold were excluded from analysis.

4. DISCUSSION

The results of this study support our hypothesis that linearization can be used to improve the repeatability of the reference region model for DCE MRI, making quantitative DCE MRI as repeatable as LTM and semi-quantitative DCE MRI. The repeatability and reproducibility of quantitative DCE MRI has been evaluated previously for the standard Tofts models and for the NRRM;[32,35,36] our work adds to this body of literature by studying the effect that linearization has on the repeatability of relative K^{trans} (R^{Ktrans}) and supporting the past study that shows linearization improves the repeatability of K^{trans}. Our Gage R&R analysis of simulations showed that a lower percentage of the variability in the measurement system is due to the algorithm when the LRRM is used instead of the NRRM, regardless of the SNR of the DCE MRI data. This is consistent with previous reports that concluded that linearization improves the accuracy of the Tofts and reference region models for DCE MRI.[24,26,] Our experimental results showed lower wSCV and *iSV* values for R^{Ktrans} with LRRM compared to NRRM, for pixelwise analyses. This improved repeatability was also evident in the pixelwise parametric maps of R^{Ktrans}. The improvement in the repeatability of the pixelwise analyses with LRRM indicated that LRRM is especially useful under conditions of lower SNR.

The wSCV for R^{Ktrans} determined by the LRRM in this study is in good agreement with the wSCV (~0.40) for R^{Ktrans} reported in previous repeatability studies of the reference region model.[34,37] However, our data was acquired at slower temporal resolution and lower SNR. The wSCV for R^{Ktrans} determined by the NRRM is only half as reproducible than previous reports, demonstrating that linearization improves the repeatability of the RRM under less-than-ideal conditions.[35,36]

PeerJ Preprints | https://doi.org/10.7287/peerj.preprints.2824v1 | CC BY 4.0 Open Access | rec: 21 Feb 2017, publ: 21 Feb 2017

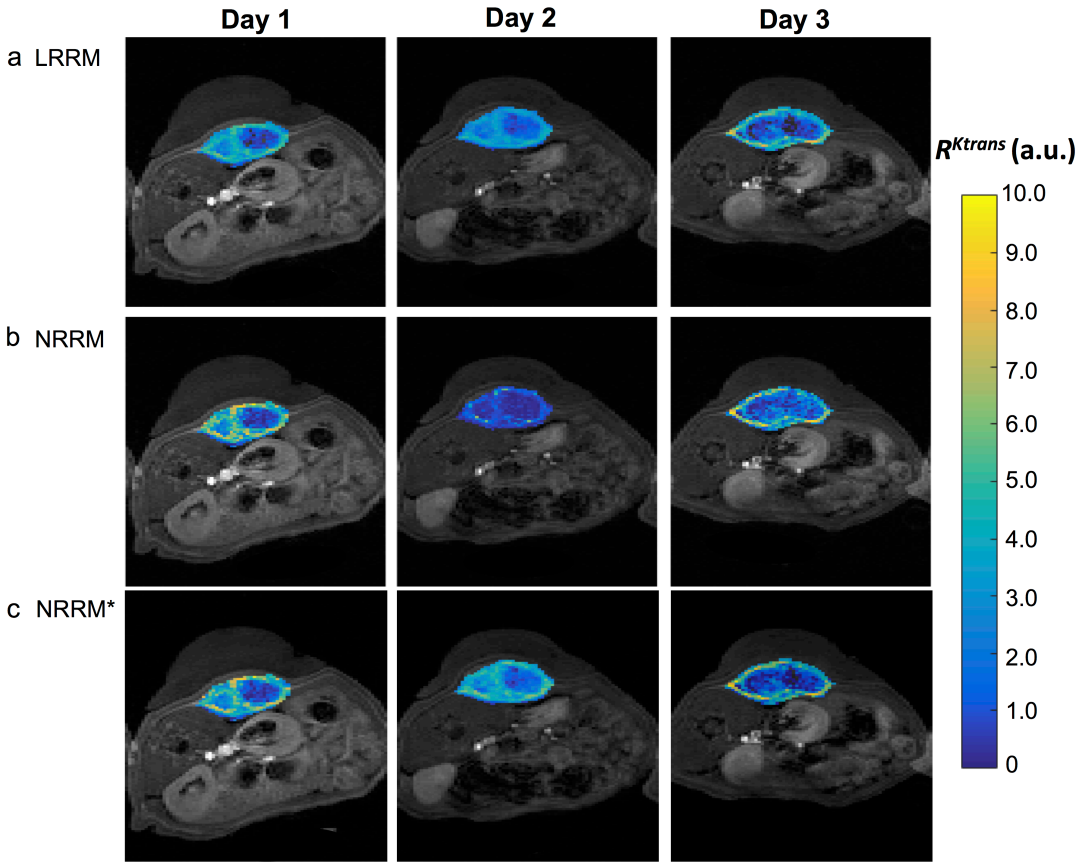

Figure 5. R^{Ktrans} parametric maps. a) LRRM b) NRRM and c) NRRM* R^{Ktrans} parametric maps of an individual rat imaged on three consecutive days.

The accuracy and precision of the algorithms most commonly used for non-linear curve fitting of DCE data are highly dependent on the initial guess of the true values of K^{trans} and k_{ep} (R^{Ktrans} for the RRM).[24,26,38] This long-standing issue in quantitative DCE MRI is either ignored or requires fitting each voxel thousands of times using different initial guesses.[37] However, this approach is computationally very demanding and does not scale linearly with the number of initial guesses. This makes quantitative DCE MRI time consuming and highly variable if the wrong initial guess is used. The linearizations of the standard Tofts model by Murase, *et al.* and the linearization of the RRM by Cárdenas-Rodríguez, *et al.*, avoid this issue entirely because their methods use a linear regression that does not require an initial guess.[24,26] Furthermore, linearization of the Tofts model (LTM) introduces a small bias into the estimated K^{trans} at slow temporal resolution and low SNR,[26] while the LRRM makes it possible to accurately estimate R^{Ktrans} at temporal resolution as slow as 30 seconds. In this study we demonstrated that the repeatability of NRRM and NTM approached the repeatability of LRRM and LTM if the results of LRRM and LTM were used as the initial guess for NRRM (NRRM*) and NTM (NTM*). Also, the median value and interquartile range of R^{Ktrans} determined using NRRM* was similar to values determined using LRRM for pixelwise analyses. This result indicated that an "ideal" initial guess can overcome the variability of NRRM analysis induced by image noise. Our

PeerJ Preprints | https://doi.org/10.7287/peerj.preprints.2824v1 | CC BY 4.0 Open Access | rec: 21 Feb 2017, publ: 21 Feb 2017

results demonstrate that the quality of NRRM analysis is fundamentally limited under practical imaging conditions.

The repeatability of R^{Ktrans} estimated with the LRRM was comparable to the repeatability of LTM, *MER* and *iauc64* measurements, as shown by Gage R&R analyses of simulated and experimental data. A previous study showed that *MER* and *iauc64* measurements have good reproducibility,[34] which suggests that LRRM also has good reproducibility (where repeatability tests measurements under the same conditions, and reproducibility tests measurements under different conditions). *TTP* measurements, R^{Ktrans} estimated with the NRRM, and K^{trans} estimated with the NTM showed the lowest repeatability, which was attributed to the stronger sensitivity to noise for these measurements.[21]

These results regarding improved repeatability and less sensitivity to image noise contribute to the evidence that LRRM has advantages relative to NRRM for DCE MRI analysis. Other studies have shown that LRRM can estimate accurate R^{Ktrans} values at temporal sampling rates as slow as 60 seconds,[24] while NRRM requires temporal sampling rates less than 32.0 seconds to estimate accurate R^{Ktrans} values,[39] and the Tofts model requires a temporal sampling rate of 5.0 seconds or faster.[15,40] Furthermore, these previous studies showed that NRRM underestimates R^{Ktrans} and overestimates $k_{ep,TOI}$ especially with low SNR, which matched the results of our study. In these previous studies, the calculation speed of LRRM was shown to be 1350-8200 times faster than NRRM (depending on the SNR).[24] For these many reasons, the LRRM is a superior approach for analyzing DCE MRI data as compared to NRRM.

Our results also demonstrate the benefits of using Gage R&R analysis as a means to compare repeatability between different MRI analysis methods. Gage R&R analysis calculates the percentage of variation due to the measurement source compared to the total variation, and thus is not subject to the scale of the DCE MRI parameter being measured. For comparison, wSCV is subject to the scale of the DCE MRI parameter, and thus wSCV is inherently smaller for DCE MRI parameters that have a small absolute value like *TTP*, compared to larger DCE MRI parameters like *MER*. In our experimental results, wSCV values for *TTP* compared to *MER* were lower, while Gage R&R analyses clearly showed better repeatability measurements for *MER* compared to *TTP*, for both pixelwise and ROI analysis, during simulations and experimental analyses.

Despite the promising results presented in this work, two limitations still remain. First, the DCE MRI data used to compare the repeatability of quantitative and semi-quantitative parameters was acquired at a temporal resolution of approximately 6.4 seconds, which is significantly faster than the standard of care for DCE MRI (20-40 seconds). Fortunately, the LRRM has been shown to be robust at low temporal resolution.[24] Second, our results were acquired in a rat model of cancer and it is still unclear if linearization also improves the repeatability of quantitative clinical DCE MRI. We have initiated clinical studies to translate our current results to diagnosis of patients.

In conclusion, this report introduces the Gage R&R analysis as a convenient method to determine the repeatability of DCE MRI, while also demonstrating that linearization increase the repeatability of the Tofts and reference region models for DCE MRI by approximately 40%.

ACKNOWLEDGEMENTS

This study was supported by the National Cancer Institute of the National Institutes of Health under award numbers R01CA167183, R01CA197029, and P30CA023074. K.M.J. is supported by a fellowship from NIH grants T32HL007955 and T32HL066988.

PeerJ Preprints | https://doi.org/10.7287/peerj.preprints.2824v1 | CC BY 4.0 Open Access | rec: 21 Feb 2017, publ: 21 Feb 2017

REFERENCES

1 Tofts PS, Brix G, Buckley DL, Evelhoch JL, et al. Estimating kinetic parameters from dynamic

2 Tofts PS, Kermode AG. Measurement of the blood-brain barrier permeability and leakage space using dynamic MR imaging. 1. Fundamental concepts. Magn Reson Med 1991;17(2):357-367.

3 De Langen AJ, Van Den Boogaart VE, Marcus JT, Lubberink M. Use of H215O-PET and DCE-MRI to measure tumor blood flow. Oncologist 2008;13(6):631-644.

4 Larsson HB, Stubgaard M, Frederiksen JL, Jensen M, Henriksen O, Paulson OB. Quantitation of blood brain barrier defect by magetic resonance imaging and gadolinium DTPA in patients with multiple sclerosis and brain tumors. Magn Reson Med 1990;16(1):117-131.

5 McDonald DM, Choyke PL. Imaging of angiogenesis: from microscope to clinic. Nature Med 2003;9(6):713-725.

6 Su MY, Wang Z, Carpenter PM, Lao X, Mühler A, Nalcioglu O. Characterization of N-ethyl-N-nitrosourea-induced malignant and benign breast tumors in rats by using three MR contrast agents. J Magn Reson Imaging 1999;9(2):177-186.

7 Langer DL, van der Kwast TH, Evans AJ, Trachtenberg J, Wilson BC, Haider MA. Prostate cancer detection with multi-parametric MRI: Logistic regression analysis of quantitative T2, diffusion-weighted imaging, and dynamic contrast-enhanced MRI. J Magn Imaging 2009;30(2):327-334.

8 Jiang F, Albert DH, Luo Y, et al. ABT-869, a multitargeted receptor tyrosine kinase inhibitor, reduces tumor microvascularity and improves vascular wall integrity in preclinical tumor models. J Pharmacol Exp Ther 2011;338:134–142.

9 Thukral A, Thomasson DM, Chow CK, et al. Inflammatory breast cancer: dynamic contrast-enhanced MR in patients receiving bevacizumab—initial experience. Radiology 2007;244:727–735.

10 Buadu LD, Murakami J, Murayama S, et al. Breast lesions: correlation of contrast medium enhancement patterns on MR images with histopathologic findings and tumor angiogenesis. Radiology 1996;200:639–649.

11 Kamoun WS, Ley CD, Farrar CT, et al. Edema control by cediranib, a vascular endothelial growth factor receptor-targeted kinase inhibitor, prolongs survival despite persistent brain tumor growth in mice. J Clin Oncol 2009;27:2542–2552.

12 Batchelor TT, Sorensen AG, di Tomaso E, et al. AZD2171, a pan-VEGF receptor tyrosine kinase inhibitor, normalizes tumor vasculature and alleviates edema in glioblastoma patients. Cancer Cell 2007;11:83–95.

13 Etxano J, Insausti LP, Elizalde A, Lopez Vega JM, Plazaola A, Martinez P. Analysis of the changes induced by bevacizumab using a high temporal resolution DCE-MRI as prognostic factors for response to further neoadjuvant chemotherapy. Acta Radiol 2015;56:1300–1307.

14 Boxerman JL, Ellingson BM. Response assessment and magnetic resonance imaging issues for clinical trials involving high-grade gliomas. Top Magn Reson Imaging 2015;24:127–136.

15 Henderson E, Rutt BK, Lee TY. Temporal sampling requirements for the tracer kinetics modeling of breast disease. Magn Reson Imaging 1998;16(9):1057-1073.

16 Calamante F, Gadian DG, Connelly A. Delay and dispersion effects in dynamic susceptibility contrast MRI: simulations using singular value decomposition. Magn Reson Med 2000;44(3):466-473.

17 Heisen M, Fan X, Buurman J, van Riel NA, Karczmar GS, ter Haar Romeny BM. The influence of temporal resolution in determining pharmacokinetic parameters from DCE-MRI data. Magn Reson Med 2010;63(3):811-816.

18 Li X, Cai Y, Moloney B, et al. Relative sensitivities of DCE-MRI pharmacokinetic parameters to arterial input function (AIF) scaling. J Magn Reson 2016;269:104-12.

19 Huang W, Chen Y, Fedorov A, Li X, et al. The impact of arterial input function determination variations on prostate dynamic contrast-enhanced magnetic resonance imaging pharmacokinetic modeling: A multicenter data analysis challenge. Tomography 2016;2(1):56-66

PeerJ Preprints | https://doi.org/10.7287/peerj.preprints.2824v1 | CC BY 4.0 Open Access | rec: 21 Feb 2017, publ: 21 Feb 2017

20 Huang W, Li X, Chen Y, Li X, et al. Variations of dynamic contrast-enhanced magnetic resonance imaging in evaluation of breast cancer therapy response: a multicenter data analysis challenge. Transl Oncol 2014;7(1):153-166.
21 Ng CS, Wei W, Bankson JA, et al. Dependence of DCE-MRI biomarker values on analysis algorithm. PloS One 2015;10(7):e0130168.
22 Yankeelov TE, Luci JJ, Lepage M, et al. Quantitative pharmacokinetic analysis of DCE-MRI data without an arterial input function: a reference region model. Magn Reson Imaging 2005;23(4):519-29.
23 Kovar DA, Lewis M, Karczmar GS. A new method for imaging perfusion and contrast extraction fraction: input functions derived from reference tissues. J Magn Reson Imaging 1998;8:1126-1134.
24 Cárdenas-Rodríguez J, Howison CM, Pagel MD. A linear algorithm of the reference region model for DCE-MRI is robust and relaxes requirements for temporal resolution. Magn Reson Imaging 2013;31(4):497-507.
25 Lee J, Cárdenas-Rodríguez J, Pagel MD, Platt S, Kent M, Zhao Q. Comparison of analytical and numerical analysis of the reference region model for DCE-MRI. Magn Reson Imaging 2014;32(7):845-53.
26 Murase K. Efficient method for calculating kinetic parameters using T1-weighted dynamic contrast-enhanced magnetic resonance imaging. Magn Reson Med 2004;51:858-62.
27 DeGrandchamp JB, Whisenant JG, Arlinghaus LR, Abramson VG, Yankeelov TE, Cárdenas-Rodríguez J. Predicting response before initiation of neoadjuvant chemotherapy in breast cancer using new methods for the analysis of dynamic contrast enhanced MRI (DCE MRI) data. SPIE Medical Imaging 2016; 9788: 978801-978810.
28 http://www.mathworks.com/help/stats/gagerr.html
29 Yang C, Karczmar GS, Medved M, Stadler WM. Multiple reference tissue method for contrast agent arterial input function estimation. Magn Reson Med 2007;58(6):1266-75.
30 Burdick RK, Borror CM, Montgomery DC. Design and Analysis of Gauge R&R Studies: Making Decisions with Confidence Intervals in Random and Mixed ANOVA Models. Philadelphia, SIAM Series on Statistics and Applied Probability; 2005.
31 Donahue KM, Weisskoff RM, Parmelee DJ, et al. Dynamic Gd-DTPA enhanced MRI measurement of tissue cell volume fraction. Magn Reson Med 1995;34:423-32.
32 Simpson NE, He Z, Evelhoch JL. Deuterium NMR tissue perfusion measurements using the tracer uptake approach: I. Optimization of methods. Magn Reson Med 1999;42:42–52.
33 Padhani AR, Hayes C, Landau S, Leach MO. Reproducibility of quantitative dynamic MRI of normal human tissues. NMR Biomed 2002;15:143-53.
34 Bland MJ, Altman DG. Statistics notes: measurement error proportional to the mean. Br Med J 1996; 313:106.
35 Galbraith SM, Lodge MA, Taylor NJ, Rustin GJ, Bentzen S, Stirling JJ, Padhani AR. Reproducibility of dynamic contrast-enhanced MRI in human muscle and tumours: comparison of quantitative and semi-quantitative analysis. NMR Biomed 2002;15(2):132-42.
36 Yankeelov TE, DeBusk LM, Billheimer DD, et al. Repeatability of a reference region model for analysis of murine DCE-MRI data at 7T. J Magn Reson Imaging 2006; 24(5):1140-7.
37 Yang C, Karczmar GS, Medved M, Oto A, Zamora M, Stadler WM. Reproducibility assessment of a multiple reference tissue method for quantitative dynamic contrast enhanced–MRI analysis. Magn Reson Med 2009; 61(4):851-9.
38 Ahearn TS, Staff RT, Redpath TW, Semple SI. The use of the Levenberg–Marquardt curve-fitting algorithm in pharmacokinetic modelling of DCE-MRI data. Phys Med Biol 2005; 50(9):N85.
39 Planey CR, Welch EB, Xu L, et al. Temporal sampling requirements for reference region modeling of DCE-MRI data in human breast cancer. J Magn Reson Imaging. 2009;30(1):121-34.
40 Evelhoch JL. Key factors in the acquisition of contrast kinetic data for oncology. J Magn Reson Imaging 1999;10(3):254-9.

PeerJ Preprints | https://doi.org/10.7287/peerj.preprints.2824v1 | CC BY 4.0 Open Access | rec: 21 Feb 2017, publ: 21 Feb 2017